Ultrasensitive organic phototransistors with multispectral response based on thin-film/single-crystal bilayer structures

R. M. Pinto' , W. Gouveia, A. I. S. Neves, and H. Alves

Articles you may be interested in

Device physics of highly sensitive thin film polyfluorene copolymer organic phototransistors
Appl. Phys. Lett. **107**, 024509024509 (2010); 10.1063/1.3273332

Ultrasensitive organic phototransistors with multispectral response based on thin-film/single-crystal bilayer structures

R. M. Pinto,[1,2,a)] W. Gouveia,[1] A. I. S. Neves,[1,3] and H. Alves[1,4]

[1]INESC MN and IN, Rua Alves Redol 9, 1000 029 Lisboa, Portugal
[2]CQFM, Instituto Superior Técnico, Av. Rovisco Pais, 1049 001 Lisboa, Portugal
[3]College of Engineering, Mathematics and Physical Sciences, University of Exeter, EX4 4QL Exeter, United Kingdom
[4]CICECO, Physics Department, Universidade de Aveiro, 3810 193 Aveiro, Portugal

We report on highly efficient organic phototransistors (OPTs) based on thin-film/single-crystal planar bilayer junctions between 5,6,11,12-tetraphenyltetracene (rubrene) and [6,6]-phenyl-C_{61}-butyric acid methyl ester ($PC_{61}BM$). The OPTs show good field-effect characteristics in the dark, with high hole-mobility (4 5 $cm^2 V^{-1} s^{-1}$), low-contact resistance (20 kΩ cm), and low-operating voltage (≤ 5 V). Excellent sensing capabilities allow for light detection in the 400 750 nm range, with photocurrent/dark current ratio as high as 4×10^4, responsivity on the order of 20 A W^{-1} at 27 μW cm^{-2}, and an external quantum efficiency of 52 000%. Photocurrent generation is attributed to enhanced electron and hole transfer at the interface between rubrene and $PC_{61}BM$, and fast response times are observed as a consequence of the high-mobility of the interfaces. The optoelectronic properties exhibited in these OPTs outperform those typically provided by a-Si based devices, enabling future applications where multifunctionality in a single-device is sought. © 2015 AIP Publishing LLC.
[http://dx.doi.org/10.1063/1.4937005]

Field-effect transistors based on organic single-crystals (SCs) have been often used as tools to investigate the intrinsic properties of organic semiconductors, due to the long-range order of the active medium.[1,2] They can serve as light-sensing optoelectronic devices termed phototransistors (OPTs), if the semiconductor comprising the active channel is photosensitive.[3] In recent years, research on OPTs has been active on bringing the best of organic materials, *application-tuned functionality*, to an increasing number of applications, e.g., light-induced switches,[4] inverters,[5] memory circuits,[6] and highly sensitive image sensors.[7] Typically, OPTs are more sensitive than photodiodes, with lower dark-levels, due to their built-in capacity of providing large signal amplification.[7] Their responsivity (R_{ph}) can be tuned by the voltage applied to source/drain/gate (S/D/G) electrodes.[6] Unlike photodiodes,[8] OPTs can reach external quantum efficiencies (EQEs) in excess[9] of 100%, with spectral coverage depending on the materials used.

To broaden the spectral response and increase charge-separation, heterojunctions (HJs) of donor and acceptor materials have been in used in OPTs.[4,5] While this strategy is common practice in organic solar cells,[10,11] its application to OPTs is still limited.[7] Devices based on solution-processed blends exhibit low charge-mobilities ($10^{-2} cm^2 V^{-1} s^{-1}$), which limit the use of OPTs as regular transistors.[4] By using single-crystals as active channels, this problem diminishes.[3] Yet, until now, SC-based OPTs have been restricted to single-layer architectures, where spectral coverage is limited by the absorption range of the one single material used.[3,6,7] To this end, further research on OPTs based on SC interfaces and bilayers is of primary importance to the development of high-performance optoelectronic devices.

In this letter, we present OPTs with an active layer comprised of SC rubrene on top of a $PC_{61}BM$ thin-film [Fig. 1]. Such OPTs operate at low-voltage (≤ 5 V), exhibit an average field-effect mobility (μ_{FE}) of 4 5 $cm^2 V^{-1} s^{-1}$, a $I_{ON/OFF}$ ratio of 10^4, and a photosensitivity (P = I_{ph}/I_d) of 10^4. They also show an extended responsivity over the entire visible region (400 750 nm) with EQE reaching 52 000%.

The fabrication of the interfaces is similar to that reported in our previous work,[12] except that here we use a Si/SiO_2 substrate and a thinner $PC_{61}BM$ layer. Prior to spin-coating a $PC_{61}BM$ solution on top of the substrate, the SiO_2 surface is cleaned by reactive ion etching (RIE) in an oxygen plasma. $PC_{61}BM$:chlorobenzene solution (20 mg ml^{-1}) is sonicated overnight ($\sim$12 h, 50 °C), filtered (0.2 μm PTFE), and spin-casted on top of heavily doped *n*-type Si substrate (5 × 20 mm) with a thermally grown 200 nm thick SiO_2 layer. The latter two act as gate electrode and gate dielectric, respectively. The substrate was held at room temperature during coating, resulting in a smooth $PC_{61}BM$ film (r.m.s. roughness = 0.7 nm), as shown in the atomic force microscopy (AFM) image in Fig. 1(a), and in the supplementary material (Fig. S1, Ref. 13) The thickness of the films was 60 90 nm, measured with a contact surface profilometer. The films were left air-dry in a laminar flow hood for $\sim$12 h before the lamination step, to minimize solvent inclusion.

Stripe-like rubrene SCs are grown by physical vapor transport[14] (PVT), under a stream of high-purity Ar, as reported before.[12,15] The selected rubrene SCs with length(L)/width(W) ratio >1 and thickness $t < 500$ nm were carefully laminated on top of the $PC_{61}BM$ layer. If channel (R_{ch}) and contact (R_c) resistances are comparable, then opting for L/W > 1 minimizes

a)Author to whom correspondence should be addressed. Electronic mail: rpinto@inesc mn.pt
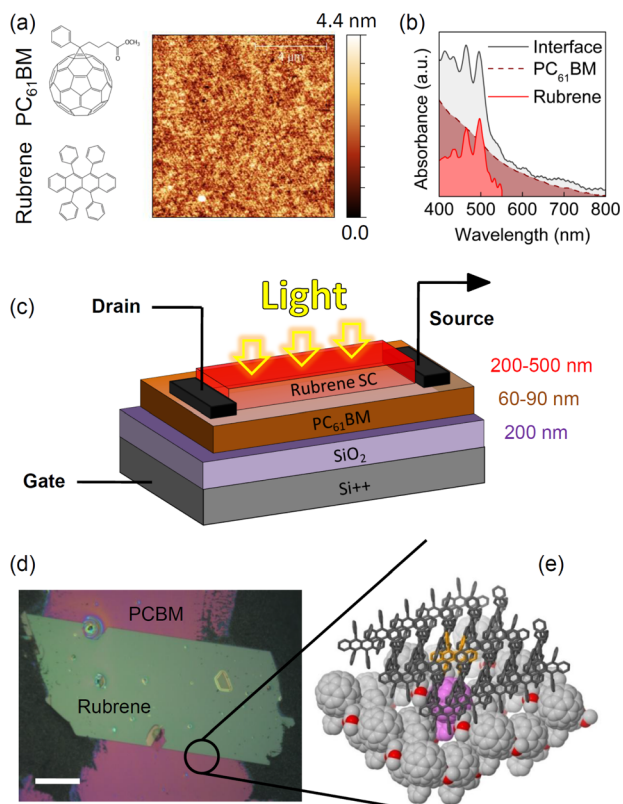
FIG. 1. (a) Chemical structure of $PC_{61}BM$ and rubrene and AFM image ($10 \times 10 \, \mu m^2$) of $PC_{61}BM$ film. (b) Absorption profile of the materials and interface used in this study. (c) Schematic representation of the $PC_{61}BM$/rubrene OPT. (d) Optical microscope image of the $PC_{61}BM$ film/rubrene single crystal interface on top of a Si/SiO_2 substrate. (e) Molecular view of the organic interface.
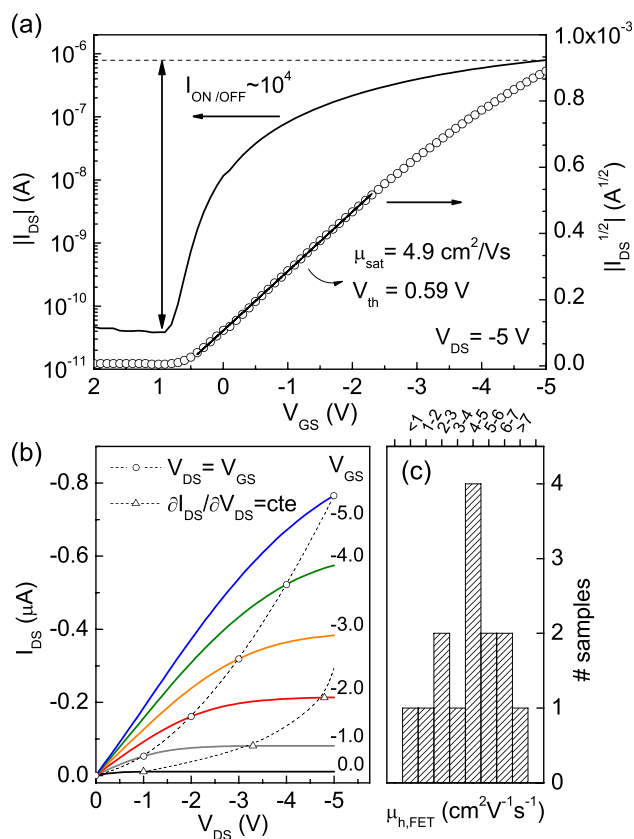

FIG. 2. (a) Transfer and (b) output characteristics measured at different gate voltages, in the dark, of a $PC_{61}BM$/rubrene OPT with $L \times W$ 260 $\times 167 \, \mu m^2$. (c) Mobility spread for $PC_{61}BM$/rubrene OPTs measured in the saturation regime.

the negative effect of contact resistance on charge-extraction, since $R_T = R_{ch} + R_c = R_s(L/W) + R_c$, where R_T and R_s are the total and sheet resistances, respectively. The crystals completely adhere to the surface of the film, guaranteeing the formation of a nanoscale interface [Figs. 1(d) and 1(e)]. The structural integrity of rubrene is preserved with lamination, and this results in a hybrid-phase bilayer junction of a crystal-line electron-donor layer (rubrene) and an amorphous acceptor layer ($PC_{61}BM$). S/D contacts are formed using a water-based carbon solution, deposited at the far edges of the interface across the long axis of crystal growth (*b*-axis). This is the axis of closest π-stacking and highest-mobility in organic field-effect transistors (OFETs) of single-crystal rubrene.[1] The resulting devices have the same bottom-gate/middle-contact (BG/MC) three-terminal configuration also found in, e.g., C_{60}/pentacene OFETs.[16] In our devices, the channel conductance can also be controlled by light irradiation [Fig. 1(c)].

Figures 2(a) and 2(b) present the transfer ($I_{DS} - V_{GS}$) and output ($I_{DS} - V_{DS}$) characteristics of a representative $PC_{61}BM$/rubrene OPT ($L = 260 \, \mu m$, $L/W \sim 1.5$) measured in the dark, under ambient conditions. The current increases with increasing negative gate voltage, typical of field-effect-induced hole conduction. This is the expected behavior for rubrene, meaning that the interface conduction is dominated by unipolar transport in the *p*-type layer. Unlike $PC_{61}BM$/pentacene thin-film based OPTs,[5] we did not observe ambipolar behavior in the $PC_{61}BM$/rubrene devices. We attribute this to the large mobility unbalance ($\mu_h > 100\mu_e$) arising

from the long-range order of the rubrene SC layer, which allows mobilities as high as $10 \, cm^2 \, V^{-1} \, s^{-1}$, in contrast to the low electron mobility observed in $PC_{61}BM$ amorphous thin-film transistors ($10^{-2} \, cm^2 \, V^{-1} \, s^{-1}$).[1,17] Note that ambipolar operation in monolithic or bilayer/heterojunction OFETs often requires lower-work function electrodes,[18,19] trap passivating layers,[5] and higher operating voltages none of which were used herein.

The mobility and threshold voltage (V_{th}) in the saturation regime ($V_{DS} > V_{GS}$) are $4.9 \, cm^2 \, V^{-1} \, s^{-1}$ and 0.59 V, respectively, calculated according to $I_{DS} = (\mu C_i W/2L)(V_{GS} - V_{th})^2$ and considering only the capacitance of the SiO_2 layer ($C_i = 17.3 \, nF \, cm^{-2}$). The OPTs exhibit low pinch-off voltages, as estimated by V_{DS} above which $\partial I_{DS}/\partial V_{DS}$ becomes constant [Fig. 2(b)].[20] The hole mobility is $5 \, cm^2 \, V^{-1} \, s^{-1}$, measured in the saturation regime, with average V_{th} of 0.67 V. The 14 devices present some dispersion due to differences in crystal quality [Fig. 2(c)]. If the capacitance of the $PC_{61}BM$ layer is added ($\epsilon_r = 3$, $t = 90 \, nm$), the average hole mobility drops to 40% of the original value ($5 \rightarrow 2 \, cm^2 \, V^{-1} \, s^{-1}$), still in line with data reported for rubrene single-crystal FETs. The non-zero threshold voltage could be related to the existence of a built-in channel, formed from partial charge-transfer between $PC_{61}BM$ and rubrene,[12] or to a non-negligible density of charge traps at the active channel/dielectric interface.[21] Overall, the performance of these devices as standard OFETs is in line with other systems based on *p*-type organic SCs, such as acenes and tetrathiafulvalene derivatives.[3,21] R_c is

$20 \, k\Omega \, cm$, extracted by the transmission line method[22] (TLM) in the linear regime, and gate dependent as presented in Fig. S2 (see Ref. [13]). This value is close to $5 \, k\Omega \, cm$ measured in bottom-gate/top-contact rubrene SC-FETs.[2]

OPT performance is analysed based on three figures-of-merit: light responsivity (R_{ph}), photosensitivity (P), and EQE. These parameters enable a normalized comparison between devices. R_{ph}, in AW^{-1}, can be defined by the following equation:[4]

$$R_{ph} = \frac{I_{ph} S_{ch}^{-1}}{E_{light}} = \frac{(I_l - I_d)(LxW)^{-1}}{P_{opt} S_b^{-1}}, \qquad (1)$$

where I_{ph} is the source-drain photocurrent, I_l and I_d are the source-drain current at fixed drain and gate voltages, under light illumination and in the dark, respectively. $E_{light} = P_{opt}/S_b$ is the irradiance of the excitation source, where P_{opt} is the optical power and S_b the excitation beam spot size (typically, $1 \, mm^2$). To enable a comparison among devices with crystals of different sizes, I_{ph} is normalized by the active (interface) channel area S_{ch}.

Figure 3(a) shows V_{th}-normalized transfer curves of a $PC_{61}BM$/rubrene OPT, in the dark and under illumination with a monochromatic green light ($\lambda = 500 \, nm$, $E_{light} \approx 16.8 \, \mu W \, mm^{-2}$). The measurement setup used for optoelectronic characterization of the OPTs is described elsewhere.[12,23] Light at 500 nm matches the maximum absorption peak of rubrene SC in the visible range (see Fig. 1(a) and Ref. [12]). Hence, photocurrent build-up in the active channel should originate from rubrene's excitons that split at the interface with $PC_{61}BM$. The large increase in current upon illumination indicates that light can act as an additional terminal that controls device operation, along with the standard S/D/G electrodes. The effect is also observed at other wavelengths in the visible range, as can be seen on Fig. 3(b) with illumination at 680 nm. However, at on-state, the difference between dark and light is less pronounced, and in the saturation regime, I_{DS} light levels rise above the dark current. The I_{DS} increase at wavelengths higher than 550 nm is due to $PC_{61}BM$ excitons evolving into free-charges via a hole transfer (HT) mechanism.[12]

When the transistor operates in accumulation mode (on-state, i.e., $V_{GS} - V_{th} < 0$ for p-type device), it presents the maximum responsivity, $\approx 20 \, AW^{-1}$, at lowest optical power [Fig. 3(a)]. A possible explanation is a photovoltaic (PV) effect, causing a P_{opt}-dependent photocurrent that can be expressed as[24]

$$I_{ph,pv} = \frac{AkT}{q} \ln \left(1 + \frac{B \eta q \lambda P_{opt}}{I_d hc} \right), \qquad (2)$$

where A and B are fitting parameters, hc/λ is the photon energy, I_d the dark current for electrons, and η the photogeneration quantum efficiency. Fittings to measured data using Eq. (2) show that I_{ph} saturates at high P_{opt} [Fig. 3(c)] values. These results indicate that $PC_{61}BM$/rubrene OPTs follow the PV effect in the turn-on state, at spectral regions (500 nm vs. 680 nm) where excitons from either p- (rubrene) or n-type ($PC_{61}BM$) materials contribute to photocurrent. In the PV effect, photogenerated holes flow to the drain electrode,
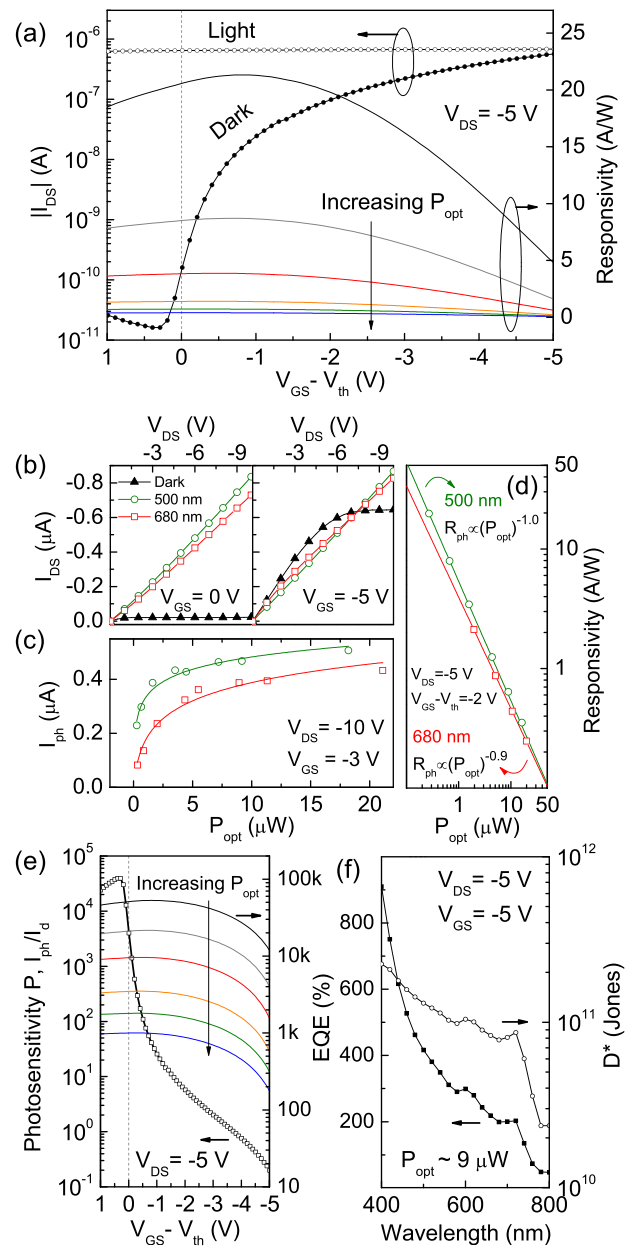

FIG. 3. (a) V_{th} normalized transfer characteristics of a $PC_{61}BM$/rubrene OPT ($L \times W$ $260 \times 167 \, \mu m^2$) measured at V_{DS} $5 \, V$, in the dark, and under green light illumination (λ $500 \, nm$, $16.3 \, \mu W$). Responsivity R_{ph} as a function V_{GS} V_{th} with increasing optical power (P_{opt} $16.8 \pm 0.3 \, \mu W$). (b) Drain current in the dark, and under 500 and 680 nm illumination, at V_{GS} 0 and $5 \, V$. (c) Photocurrent and (d) responsivity as a function of P_{opt}. (e) Photosensitivity P as a function of V_{GS} V_{th}, and EQE dependence on gate voltage and P_{opt}. (f) EQE and specific detectivity D* over 400   800 nm, under strong irradiance (E_{light} $0.9 \, mW \, cm^{-2}$).

while negative charges accumulate under the source electrode, reducing the barrier height for hole injection and, thus, the contact resistance.[24] This leads to a positive shift in V_{th}.

At 680 nm, there is a sublinear dependence of R_{ph} on P_{opt}, i.e., $R_{ph} \propto P^{-0.9}$, which likely comes from enhanced singlet-singlet exciton annihilation, due to higher density of photogenerated excitons at increasing optical power [Fig. 3(d)]. The photosensitivity (or photoswitching ratio) for a typical $PC_{61}BM$/rubrene OPT, defined as $P = I_{ph}/I_d$, peaks at 4×10^4 under 500 nm light illumination, near $V_{GS} - V_{th} = 0$ in the off-state of the transistor, as displayed in Fig. 3(e).

Similarly to other p-type OPTs, photosensitivity decreases with more negative V_{GS}, owing to the large drain current already flowing through the channel without illumination. Increasing P_{opt} leads to negligible changes in photosensitivity; therefore, P is almost independent of light power.

Also, in Fig. 3(e), EQE is presented, which takes only into account the electronic processes in the device and is related to R_{ph} as EQE $= (hc/\lambda q)R_{ph}$. At low irradiance values ($E_{light} = 27\,\mu W\,cm^{-2}$, 500 nm), EQE reaches 52 900%. This value is almost $20\times$ higher than the gain observed for high-quality n^+p photodiodes ($>3000\%$).[25] It can be attributed to the existence of a photomultiplication (PM) mechanism, and to the low charge-recombination due to the defect-free nature of rubrene SCs. Under stronger irradiance ($E_{light} = 0.9\,mW\,cm^{-2}$), EQE is 900% at 400 nm and follows the absorption profile of the interface up to ca. 700 nm, and then steeply goes below 100%, signaling the absence of a PM mechanism [Fig. 3(f)]. The onset of the EQE spectrum occurs right at the onset of absorbance for the film/single-crystal interface shown in Fig. 1(b), as observed before.[12] Specific detectivity (D^*) is 1.2×10^{11} Jones, calculated using $D^* = R_{ph}/\sqrt{2eI_d/S_{ch}}$, where e is the electron charge, R_{ph} is responsivity, I_d the dark current for electrons, and S_{ch} is the device area. Shot noise from dark current was assumed as the dominant contribution over Johnson, dielectric or flicker noise.[26]

In OPTs, PM-based EQEs in excess of 100% can have multiple origins, e.g., (i) singlet-fission, (ii) impact ionization by hot carriers, or (iii) enhanced injection via trap-assisted tunneling (TAT).[9,27,28] Singlet-fission implies very energetic photons, while impact ionization is hindered by large exciton binding energies of organic materials. However, PM via TAT injection of charges has been reported for polymer:fullerene diodes[28] and nanowire OPTs[9] with EQEs well above 100%. A possible explanation for the high EQE in our devices can be described as follows. Illumination in the off-state leads to photogenerated excitons in rubrene SC that diffuse towards the organic/organic (O/O) interface. There they split driven by an electrical field due to intrinsic interfacial band bending,[12] aided by the transversal gate-field. Holes drift to the drain, while remnant electrons fill interfacial trap states, creating a Coulomb field[27] that could further enhance exciton splitting. Ohmic contacts ensure electrical neutrality; thus, more holes will be injected for each collection-trapping event until recombination occurs. The OPT operates as a photoconductor under the effect of a transversal field, and the PM gain scales with the ratio between recombination and hole transit time.[7] Further support for the transversal field effect on the gain mechanism is given in Fig. S3 (see Ref. 13), showing an increase in EQE with decreasing channel length. In the on-state, photogenerated carriers in rubrene will add to the current already being injected into the channel. The LUMO offset[12] between rubrene ($-2.7\,eV$) and $PC_{61}BM$ ($-3.7\,eV$) provides deep electron traps ($\approx 1\,eV$) at the O/O interface.[28] Trapped electrons will also accumulate under the source, reducing the hole-tunneling injection barrier to rubrene. This TAT mechanism adds to the PV effect to further enhance charge injection. TAT should also occur for $PC_{61}BM$ excitons only ($>550\,nm$), but their lower diffusion length ($L_D \approx 5\,nm$) decreases the splitting efficiency

and the EQE. While these mechanisms already define a route to achieve very high photomultiplication gain, control experiments on devices with different configurations (e.g., top-gate) should be included in future studies.

The dynamic response of an average mobility OPT ($L \times W = 468 \times 239\,\mu m^2$, $\mu_{FE} = 4.5\,cm^2\,V^{-1}\,s^{-1}$) is displayed in Fig. 4(a), showing multispectral photoresponse from 450 to 750 nm, with P as high as 3.1×10^4 when a gate-reset pulse is used. This broad spectral response, which covers the entire visible range and extends into the NIR, is a consequence of enhanced electron (ET) and HT in the active layer. While this strategy is frequently used to exploit excitons from both organic materials in donor-acceptor (p-n) junctions in organic solar cells,[29] here we show that it can also be applied to OPTs to achieve multispectral response. A closer look at the photocurrent dynamics reveals fast rise times, $\tau_r < 0.5\,s$, and slow single exponential decays, $\tau_d \approx 4.0$–$5.5\,s$ [Figs. 4(b) and 4(c)]. These values are similar to the corresponding τ_r and τ_d reported for hybrid graphene-quantum dots photodetectors,[26] while τ_r is $10\times$ faster than that of recently developed MoS_2 light sensors.[30] They also represent a large improvement over OPTs based on amorphous oxide semiconductors, where persistent photoconductivity (PPC) can last for several hours or days.[31] As reported for other OPTs, τ_d can be improved to less than 0.5 s (i.e., the temporal resolution of our setup) by applying a short gate pulse (2s, $V_{GS} = -10\,V$), which causes a full release of
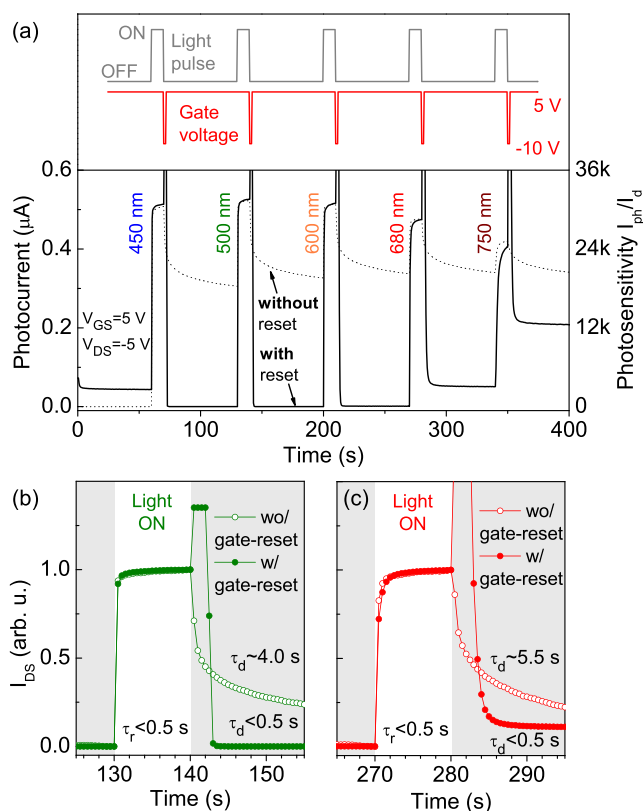

FIG. 4. (a) OPTs photoresponse switching behavior with different excitation wavelengths (λ 450, 500, 600, 680, and 750 nm, $P_{opt} \approx 7\,\mu W$), in the off state. A reset voltage pulse, V_{GS} $-10\,V$, is applied after illumination, during 2 s, to release trapped charge carriers. Time resolved photosensitivity with (b) green and (c) red light, showing decay times τ_d of 4.0 and 5.5 s (without gate reset), and $<0.5\,s$ (with gate reset), respectively, and rise time of τ_r faster than 500 ms.

trapped charge carriers.[3,26,30] This mode of operation yields lower dark currents, allowing higher detectivity (7 9 × 10^{12} Jones) than that from on-state operation.

In conclusion, OPTs based on single-crystal rubrene laminated onto $PC_{61}BM$ films show an average hole mobility in the dark of 4 5 cm^{2}V^{-1}s^{-1}, and an EQE that reaches 52 000% under low power light irradiation (500 nm, 27 μW cm^{-2}). Response over a wide spectral range (vis-NIR) with photosensitivity P as high as $4 × 10^4$ is achieved by grasping the potential of both *p*- and *n*-type materials, whose primary excitons contribute to photocurrent build-up via electron and hole-transfer mechanisms, respectively. These characteristics show the potential of bilayer organic interfaces based on materials with contrasting structural phases (single-crystal vs. amorphous) to be used in high-quality optoelectronic applications.

[1]E. Menard, V. Podzorov, S. H. Hur, A. Gaur, M. E. Gershenson, and J. A. Rogers, Adv. Mater. **16**, 2097 (2004).

[2]I. N. Hulea, S. Russo, A. Molinari, and A. F. Morpurgo, Appl. Phys. Lett. **88**, 113512 (2006).

[3]M. Mas Torrent, P. Hadley, N. Crivillers, J. Veciana, and C. Rovira, Chem. Phys. Chem. **7**, 86 (2006).

[4]N. Marjanović, T. B. Singh, G. Dennler, S. Gunes, H. Neugebauer, N. Sariciftci, R. Schwodiauer, and S. Bauer, Org. Electron. **7**, 188 (2006).

[5]J. Labram, P. Wobkenberg, D. Bradley, and T. Anthopoulos, Org. Electron. **11**, 1250 (2010).

[6]K. H. Kim, S. Y. Bae, Y. S. Kim, J. A. Hur, M. H. Hoang, T. W. Lee, M. J. Cho, Y. Kim, M. Kim, J. I. Jin, S. J. Kim, K. Lee, S. J. Lee, and D. H. Choi, Adv. Mater. **23**, 3095 (2011).

[7]K. J. Baeg, M. Binda, D. Natali, M. Caironi, and Y. Y. Noh, Adv. Mater. **25**, 4267 (2013).

[8]J. D. Zimmerman, V. V. Diev, K. Hanson, R. R. Lunt, E. K. Yu, M. E. Thompson, and S. R. Forrest, Adv. Mater. **22**, 2780 (2010).

[9]H. Yu, Z. Bao, and J. H. Oh, Adv. Funct. Mater. **23**, 629 (2013).

[10]F. Yang, M. Shtein, and S. R. Forrest, Nat. Mater. **4**, 37 (2005).

[11]W. Ma, C. Yang, X. Gong, K. Lee, and A. J. Heeger, Adv. Funct. Mater. **15**, 1617 (2005).

[12]R. M. Pinto, E. M. Maçôas, and H. Alves, J. Mater. Chem. C **2**, 3639 (2014).

[13]See supplementary material at http://dx.doi.org/10.1063/1.4937005 for details on S1: AFM measurements, S2: contact resistance extraction, and S3: EQE behavior with channel length.

[14]R. Laudise, C. Kloc, P. Simpkins, and T. Siegrist, J. Cryst. Growth **187**, 449 (1998).

[15]H. Alves, R. M. Pinto, and E. S. Maçôas, Nature Commun. **4**, 1842 (2013).

[16]E. Kuwahara, Y. Kubozono, T. Hosokawa, T. Nagano, K. Masunari, and A. Fujiwara, Appl. Phys. Lett. **85**, 4765 (2004).

[17]M. Chikamatsu, S. Nagamatsu, Y. Yoshida, K. Saito, K. Yase, and K. Kikuchi, Appl. Phys. Lett. **87**, 203504 (2005).

[18]S. Z. Bisri, T. Takenobu, T. Takahashi, and Y. Iwasa, Appl. Phys. Lett. **96**, 183304 (2010).

[19]T. Uemura, M. Yamagishi, Y. Okada, K. Nakayama, M. Yoshizumi, M. Uno, and J. Takeya, Adv. Mater. **22**, 3938 (2010).

[20]M. Imakawa, K. Sawabe, Y. Yomogida, Y. Iwasa, and T. Takenobu, Appl. Phys. Lett. **99**, 233301 (2011).

[21]R. de Boer, M. Gershenson, A. Morpurgo, and V. Podzorov, Phys. Status Solidi A **201**, 1302 (2004).

[22]Y. Xu, R. Gwoziecki, I. Chartier, R. Coppard, F. Balestra, and G. Ghibaudo, Appl. Phys. Lett. **97**, 063302 (2010).

[23]R. M. Pinto, E. M. S. Macoas, A. I. Neves, S. Raja, C. M. Baleizao, I. C. Santos, and H. Alves, J. Am. Chem. Soc. **137**, 7104 (2015).

[24]C. Choi, H. Kang, W. Y. Choi, H. Kim, W. Choi, D. Kim, K. Jang, and K. Seo, IEEE Photonics Technol. Lett. **15**, 846 (2003).

[25]A. J. Said, D. Recht, J. T. Sullivan, J. M. Warrender, T. Buonassisi, P. D. Persans, and M. J. Aziz, Appl. Phys. Lett. **99**, 073503 (2011).

[26]G. Konstantatos, M. Badioli, L. Gaudreau, J. Osmond, M. Bernechea, F. P. G. de Arquer, F. Gatti, and F. H. Koppens, Nat. Nanotechnol. **7**, 363 (2012).

[27]M. Hiramoto, K. Nakayama, I. Sato, H. Kumaoka, and M. Yokoyama, Thin Solid Films **331**, 71 (1998).

[28]W. Wang, F. Zhang, L. Li, M. Zhang, Q. An, J. Wang, and Q. Sun, J. Mater. Chem. C **3**, 7386 (2015).

[29]J. D. Douglas, M. S. Chen, J. R. Niskala, O. P. Lee, A. T. Yiu, E. P. Young, and J. M. Fréchet, Adv. Mater. **26**, 4313 (2014).

[30]O. Lopez Sanchez, D. Lembke, M. Kayci, A. Radenovic, and A. Kis, Nat. Nanotechnol. **8**, 497 (2013).

[31]S. Jeon, S. E. Ahn, I. Song, C. J. Kim, U. I. Chung, E. Lee, I. Yoo, A. Nathan, S. Lee, J. Robertson *et al.*, Nat. Mater. **11**, 301 (2012).